JOURNAL OF PETROLOGY | VOLUME 50 | NUMBER 12 | PAGES 2287–2305 | 2009 | doi:10.1093/petrology/egp076

Microcrysts Record Transient Convection at Piton de la Fournaise Volcano (La Réunion Hotspot)

BENOÎT WELSCH[1]*, FRANÇOIS FAURE[2], PATRICK BACHÈLERY[1] AND VINCENT FAMIN[1]

[1]UNIVERSITÉ DE LA RÉUNION, LABORATOIRE GÉOSCIENCES RÉUNION, UMR-CNRS 7154 IPGP, 15 AVENUE RENÉ CASSIN, 97715 SAINT-DENIS, MESSAG CEDEX 9, LA RÉUNION

[2]NANCY UNIVERSITÉ, CNRS/INSU CENTRE DE RECHERCHES PÉTROGRAPHIQUES ET GÉOCHIMIQUES, 15 RUE NOTRE DAME DES PAUVRES, 54501 VANDOEUVRE-LÈS-NANCY, FRANCE

RECEIVED DECEMBER 2, 2008; ACCEPTED OCTOBER 22, 2009
ADVANCE ACCESS PUBLICATION DECEMBER 14, 2009

We studied the morphologies of olivine, clinopyroxene and plagioclase microcrysts in olivine-rich basalts from the December 2005 eruption at Piton de la Fournaise, to reconstruct the thermal history of the magma prior to reaching the surface. Olivine microcrysts and their melt inclusions show textural and compositional evidence for rapid growth caused by successive cooling and reheating cycles below the liquidus of olivine (1230°C). Clinopyroxene crystals are corroded, which indicates reheating above the liquidus of clinopyroxene (1140°C). Clinopyroxene crystallization–dissolution is also evidenced by the composition of melt inclusions in olivine microcrysts. We interpret the cooling–heating cycles experienced by olivine and clinopyroxene microcrysts as evidence for thermal convection in the shallow magma storage zone (2–2·5 km depth) of the volcano. Plagioclase microcrysts do not record temperature fluctuations, and hence probably crystallized in the conduit. Given the small size of the olivine and clinopyroxene microcrysts and their rapid growth, it is likely that convection preceded the December 2005 eruption by only a few days at most. Our results suggest that convection is transient and proceeds in small-scale cells at low Rayleigh number ($<10^4$), rather than vigorous and continuous convection at high Rayleigh number.

KEY WORDS: *convection; crystal morphology; magma chamber; melt inclusion*

INTRODUCTION

An important goal of volcanology is to constrain the thermodynamic parameters of magmatic systems, so as to understand their evolution and to predict eruptions. In particular, a large number of experimental studies (e.g. Kushiro, 1978; Scarfe & Cronin, 1986; Richet *et al.*, 2000) have focused on the variations in density of magmas, because density is probably one of the most important parameters driving the ascent of melts or their stagnation at different levels in the Earth's mantle and crust. Magma density is influenced by temperature variations and by chemical processes such as crystallization or dissolution of minerals (e.g. Sparks & Huppert, 1984) or gas exsolution (e.g. Kazahaya *et al.*, 1994; Allard, 1997; Stevenson & Blake, 1998). For any viscous liquid, including magmas, buoyancy forces may cause instabilities if the denser liquids lie above the less dense ones. Because magmas are generally heated from below and crystallize from above, density inversion is prone to be sustained in most magmatic systems, and may lead to convection (e.g. Jaupart & Parsons, 1985). Convection occurs when the buoyancy forces are large enough to overcome viscous drag and conductive cooling effects, and when the cause of the density inversion is maintained. The vigour of convection is

*Corresponding author. Telephone: (+262) 262 97 82 10, Fax: (+262) 262 97 82 66. E-mail: benoit.welsch@univ-reunion.fr

determined by the magnitude of the Rayleigh number (Ra, dimensionless):

$$\mathrm{Ra} = \frac{\alpha g \Delta T d^3 \rho}{\mu K}$$

where α is the coefficient of thermal expansion (K^{-1}), g the gravitational acceleration (m/s^2), ΔT the temperature difference in the fluid layer (K), d the thickness of the fluid layer (m), ρ the fluid density (kg/m^3), μ the dynamic viscosity (Pa s) and K the thermal diffusivity (m^2/s).

A first possibility is that convection involves the whole thickness of the magma chamber. In this case, very large Rayleigh numbers are obtained ($\geq 10^4$) for any reasonable values of temperature gradients (10–100°C) and chamber dimensions (0·1–10 km). This has led to the conclusion that most magmas chambers are in the vigorously turbulent regime throughout their entire lifetime, especially for low-viscosity magmas such as basalts ($\alpha = 10^{-5}$ K^{-1}, $\rho = 2600$ kg/m^3, $\mu = 10$–1000 Pa s and $K = 10^{-6}$ m^2/s). However, Marsh (1989) has suggested that convection may be self-regulated at lower Rayleigh numbers by the kinetics of crystallization in the chamber, inducing complex viscosity variations. If so, convection would be a transient and small-scale process, triggered only when the cooler, denser boundary layer containing more than 50% solids at the roof of the chamber exceeds a minimum thickness (independently of the size of the reservoir and its temperature difference with the wall-rock). Once this critical thickness is reached, the crystal-rich boundary layer sinks and generates transient instabilities leading to small convection cells in the vicinity of the roof. To date, there is no evidence on whether natural magma chambers undergo continuous versus short-lived convection, because this dynamics is instantaneous at the geological timescale, and is hard to assess with geophysical or geochemical approaches.

In this study, we investigate the thermal history of basaltic magma prior to the December 2005 eruption at Piton de la Fournaise volcano (La Réunion Island). The originality of our approach is to use microcrysts contained in the groundmass of the lavas. Microcrysts have received little attention except in a few recent studies (e.g. Martel *et al.*, 2006; Guilbaud *et al.*, 2007) because they are traditionally interpreted as having crystallized during the solidification of the magma at the surface. However, a closer look allows the distinction between microcrysts crystallized on the surface from those crystallized deeper. The shape of microcrysts is known to depend largely on the magnitude and rate of temperature variations during their crystallization; recent experimental studies (Faure *et al.*, 2003*a*, 2003*b*) have classified crystal shapes to constrain these temperature variations. Taking advantage of this property, we describe the different morphologies of the microcrysts and use them as probes of thermal variations in the chamber. Our textural observation of microcrysts from Piton de la Fournaise products has critical implications for the dynamics of convection in a magma chamber.

BACKGROUND

La Réunion Island is made of two main volcanoes: Piton des Neiges, whose activity started in Pliocene times and ended 12 kyr ago (McDougall, 1971; Deniel *et al.*, 1992), and Piton de la Fournaise, which has been active since 530 ka (Gillot & Nativel, 1989). The most frequently erupted products at Piton de la Fournaise are 'Steady State Basalts' (49–50 wt % SiO_2; 5–7 wt % MgO; 10–12 wt % CaO; 0·7–0·9 wt % K_2O, Albarède *et al.*, 1997), flowing in small volumes ($0{\cdot}1$–10^5-10^7 m^3) from vents located near the summit cone at temperatures of 1150–1170°C (Coppola *et al.*, 2007; Boivin & Bachèlery, 2009). Less frequent eruptions of picrobasalts and picrites with 8–28 wt % MgO (those with more than 20 wt % are referred to as 'oceanites,' Lacroix, 1923) are also observed in large volumes ($>10^7$ m^3) erupting from vents located on the lower parts of the volcano slopes. The picrites, picrobasalts and Steady State Basalts have similar matrix glass compositions and their bulk-rock compositions plot on an olivine control line consistent with olivine accumulation (Boivin & Bachèlery, 2009). Albarède *et al.* (1997) demonstrated the fractionation of olivine and clinopyroxene from the basalts without significant contribution of plagioclase. Vlastélic *et al.* (2007) identified a temporal increase in the CaO/Al_2O_3 ratio of bulk lavas erupted over the period 1998–2006 (Fig. 1a). This increase is continuous over time once the inter-eruptive periods are removed (Fig. 1b), which led Vlastélic *et al.* to the conclusion that the magmas become enriched during eruptions by removing clinopyroxene from the conduit.

Based on ground deformations and the location of earthquakes swarms, at least three reservoirs have been evidenced at Piton de la Fournaise (Aki & Ferrazzini, 2000): (1) a deep reservoir located beneath the oceanic crust at ~12 km below sea level (b.s.l.) (Cayol & Cornet, 1998; Sigmundsson *et al.*, 1999); (2) an intermediate reservoir at 5 km b.s.l. (Battaglia & Bachèlery, 2003; Battaglia *et al.*, 2005*b*; Fukushima *et al.*, 2005); (3) a shallow reservoir at ~0·5 above sea level (a.s.l.); that is, 2–2·5 km beneath the summit (Lénat & Bachèlery, 1990; Nercessian *et al.*, 1996; Sapin *et al.*, 1996; Battaglia *et al.*, 2005*a*; Peltier *et al.*, 2005). The shallow reservoir has been shown to constitute an important growth zone for olivine macrocrysts (Famin *et al.*, 2009). It has been re-supplied during March 1998 (Battaglia & Bachèlery, 2003), from the middle of 2001 to December 2002 (Vlastélic *et al.*, 2005; Peltier *et al.*, 2007), during February 2005 (Vlastélic *et al.*, 2007), October 2005 (Peltier *et al.*, 2008) and the first half of 2006 (Coppola *et al.*, 2009). Importantly, there was no evidence of a refilling event during the December 2005 eruption.

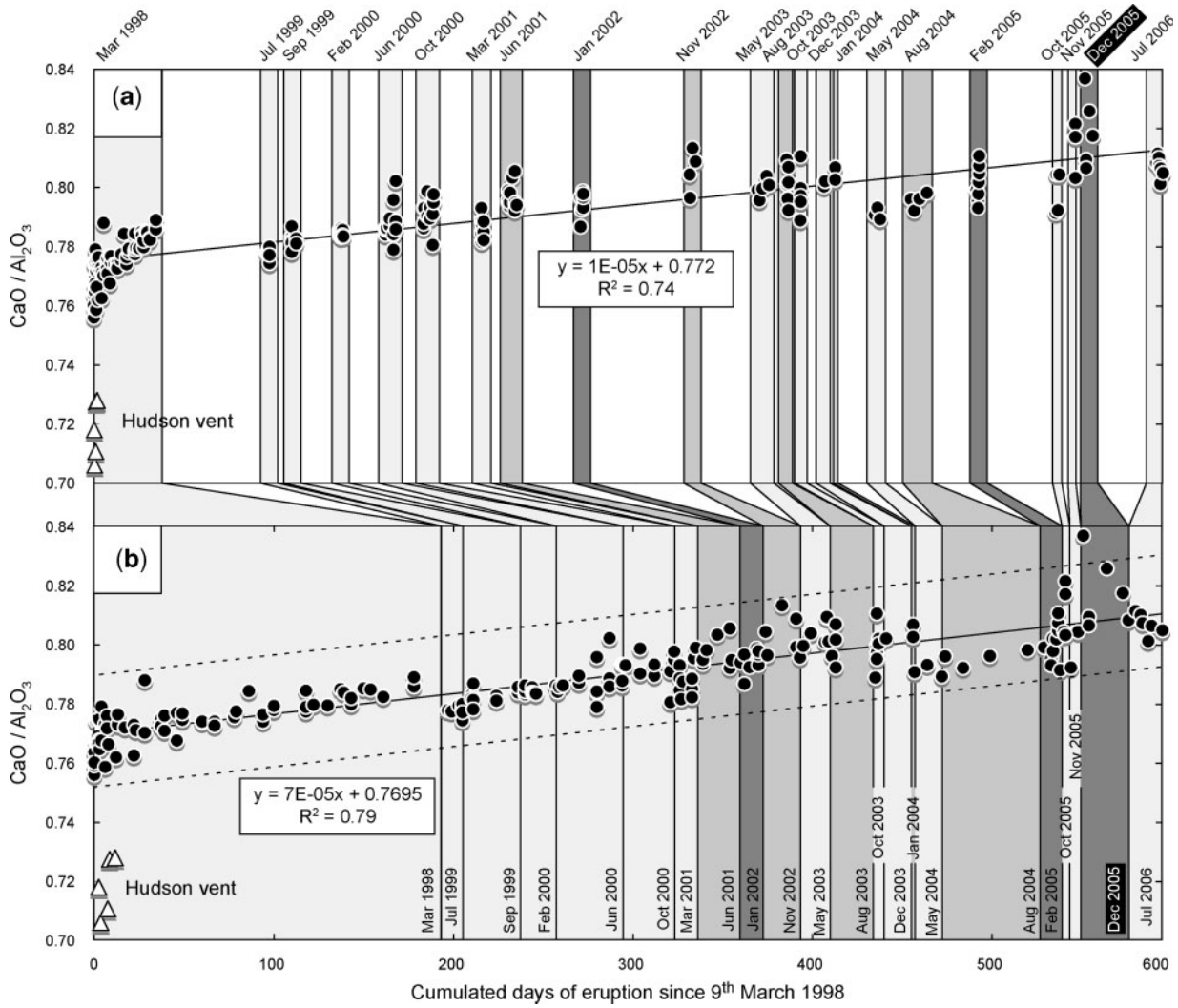

Fig. 1. CaO/Al_2O_3 variations in bulk lavas from 9 March 1998 to 8 August 2006 plotted against (a) time and (b) cumulative eruption duration. Modified after Vlastélic *et al.* (2007). Eruptions are shaded in light grey for aphyric basalts (6–7 wt % MgO), medium grey for picrobasalts and picrites (8–20 wt % MgO) and dark grey for oceanites (>20 wt % MgO). Most eruptions were accompanied by seismic activity in the shallow magma storage zone located at 2–2·5 km depth. The magma erupted on March 1998 at Hudson vent is assumed to have a deeper origin (Bureau *et al.*, 1998, 1999; Battaglia *et al.*, 2005*b*).

Monitoring of the recent activity indicates that most of the eruptions, including the December 2005 eruption, come from the shallow reservoir.

The December 2005 eruption was preceded by 2 months of increasing seismic activity at low intensity (fewer than 120 events per day) in the shallow storage zone (Peltier *et al.*, 2008). On 26 December at 10:45 UTC, a strong crisis of more than 900 events occurred at the roof of the shallow reservoir. Ground deformation indicated the lateral propagation of a dyke from the eastern side of the roof of the chamber. The magma reached the surface at 13:00 UTC and effused in small volumes near the summit cone. At 19:55 UTC, a new fissure opened on the northern side of the Enclos Fouqué caldera, at 4·3 km NNE of the summit and 1·6 km a.s.l. (Fig. 2). The effusions from this vent ended 24 days later on 18 January 2006. The total volume of erupted magma was estimated to be 1.5×10^7 m^3.

SAMPLING AND ANALYTICAL TECHNIQUES

Four samples were collected on days 2, 5, 15 and 24 of the December 2005 eruption, 1 km downstream of the vent (Fig. 2). Samples from days 2 and 5 were naturally cooled in air, whereas samples from days 15 and 24 were quenched in water. In addition, lapilli (Ø 5–50 mm; Ø represents

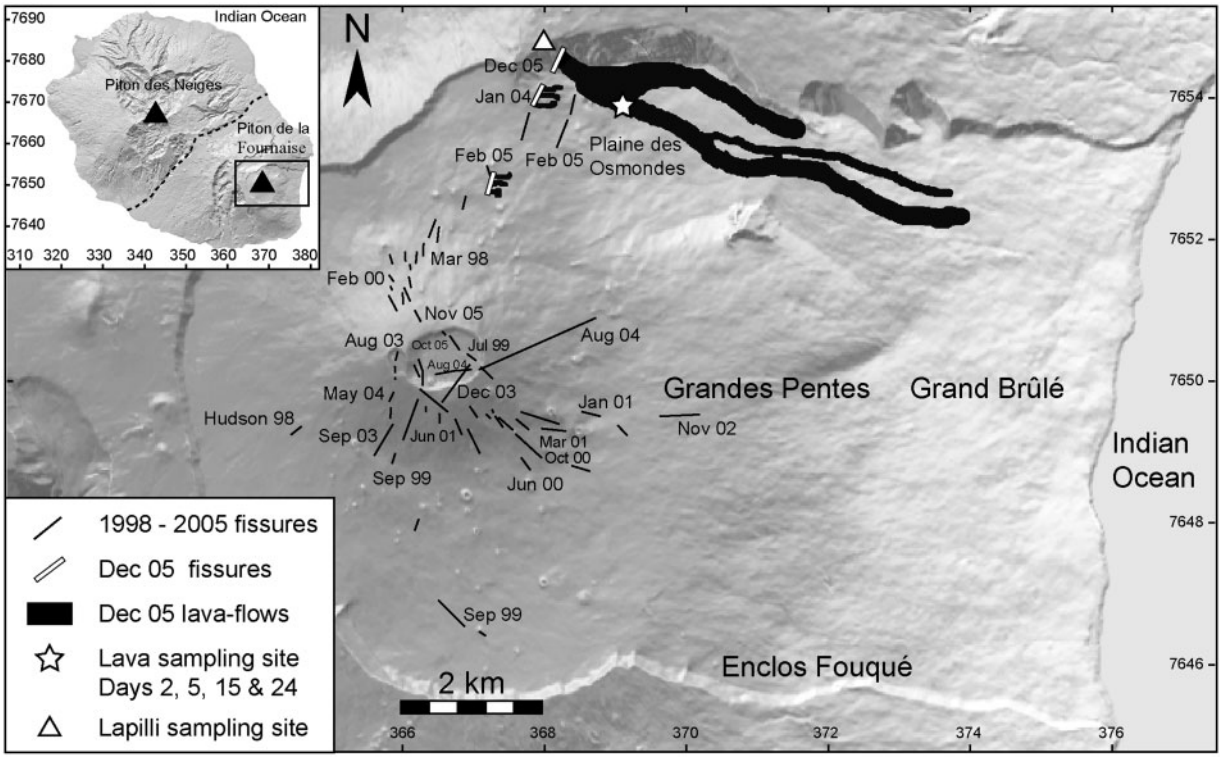

Fig. 2. Map of the December 2005 eruption at Piton de la Fournaise (La Réunion Island). Most eruptions during the period 1998–2005 started with magma intrusion into the shallow storage zone (2–2·5 km beneath the summit cone), which propagated in a dyke at 0·2–2 m/s (Battaglia & Bachèlery, 2003; Peltier *et al.*, 2005, 2007; see also Toutain *et al.*, 1992). Lavas erupted from new fissures opened along N30 or N130 trends (Michon *et al.*, 2007; Letourneur *et al.*, 2008).

the maximum dimension) were collected around the vent after the eruption. Samples were mounted in epoxy and prepared as polished thin sections for optical microscopic examination. Major element compositions of the different phases were determined using a CAMECA SX-100 electron probe micro-analyser at Nancy University (France), at 15 kV voltage, 10 nA current and 10 s peak counting time (Na measured first). Natural and synthetic mineral standards were used for calibration: orthoclase (Si, K), albite (Na, Al), wollastonite (Ca), hematite (Fe), olivine (Mg), pyrophanite (Ti, Mn), NiO (Ni), $KTi_2(PO_4)_3$ (P), Cr_2O_3 (Cr). Minerals were analysed with the beam focused at 1–2 μm. Because of their tiny size ($Ø < 10$ μm), melt inclusions were also analysed with a focused beam, with the possible drawback of alkali loss. Matrix glasses were analysed with a beam defocused to 20 μm to reduce alkali loss. Melt inclusions were not re-homogenized before analysis, and no correction for possible post-entrapment chemical changes (epitaxial crystallization or iron loss by diffusion) was applied. Analytical uncertainty (1σ) is 1–2% for major elements, 5–15% for minor elements and 50–100% for trace elements. Detection limit is in the range 0·05–0·15 wt % for CaO, K_2O, TiO_2, P_2O_5 and Cr_2O_3, and 0·15–0·2 wt % for SiO_2, Al_2O_3, FeOt, MnO, MgO, Na_2O and NiO.

PETROGRAPHY

A striking feature of the December 2005 eruption is the increasing MgO content in lavas with increasing eruption duration (Peltier *et al.*, 2008). For example, samples from days 2 and 5 are transitional picrobasalts with 9–12 wt % MgO (Le Bas, 2000) and samples from days 15 and 24 are oceanites with up to 26 wt % MgO (Table 1). Lapilli consist of vesicular glassy fragments or olivine grains coated with a film of glass. All of the lava samples contain macrocrysts ($Ø > 0·5$ mm), mesocrysts (Ø 0·1–0·5 mm) and vesicles in a groundmass of glass and microcrysts ($Ø < 0·1$ mm). We use the terms 'macrocryst', 'mesocryst' and 'microcryst' rather than 'phenocryst', 'microphenocryst' and 'microlite' because these terms are strictly descriptive and devoid of petrogenetic interpretation. Macrocrysts are exclusively of olivine, mesocrysts are either olivine or an assemblage of clinopyroxene + plagioclase, and microcrysts are olivine + clinopyroxene + plagioclase + Cr-spinel ± Fe–Ti oxide (Fig. 3a–h). In addition to their grain size, each crystal population has specific textures, core compositions and/or types of inclusions.

Macrocrysts and mesocrysts

Olivine macrocrysts exhibit the typical compositional and petrographic features of picrite olivine, described in

Table 1: *Bulk compositions of lava samples collected throughout the December 2005 eruption*

Day:	2	5		18	24
Sample:	0512-271	0512-301	0512-303	0601-091	0601-181
SiO_2	47·06	48·28	48·34	43·70	43·53
Al_2O_3	12·21	13·44	13·34	7·64	7·07
Fe_2O_3	13·36	12·91	12·89	14·31	14·63
MnO	0·18	0·18	0·18	0·19	0·19
MgO	12·10	9·04	9·44	24·52	26·4
CaO	10·22	10·88	10·76	6·31	5·78
Na_2O	2·35	2·61	2·60	1·49	1·33
K_2O	0·61	0·65	0·64	0·34	0·30
TiO_2	2·36	2·62	2·59	1·48	1·37
P_2O_5	0·28	0·32	0·31	0·18	0·17
LOI	−0·51	−0·85	−0·57	−0·62	−0·45
Total	100·31	100·15	100·63	99·57	100·31
CaO/Al_2O_3	0·84	0·81	0·81	0·83	0·82
K_2O/TiO_2	0·26	0·25	0·25	0·23	0·22

From Vlastélic *et al.* (2007). LOI, loss on ignition.

previous studies (Clochiatti *et al.*, 1979; Albarède & Tamagnan, 1988; Bureau *et al.*, 1998; Famin *et al.*, 2009). They have a homogeneous core composition ($Fo_{85–83}$) and a 10 μm thick edge ($Fo_{82–79}$; Fig. 4, Table 2). Most macrocrysts are polyhedral (i.e. with a simple polygonal shape; Fig. 3a) with occasional kink-bands. They contain euhedral Cr-spinel crystals (Table 2), primary melt inclusions and planes of secondary melt and fluid inclusions.

Olivine mesocrysts have a larger range of core compositions ($Fo_{85–81}$) with edges of $Fo_{82–79}$ (Fig. 4, Table 2). They often appear as clusters of several grains. Olivine mesocrysts are polyhedral or skeletal (i.e. a polygonal shape with cavities) with occasional 50–200 μm long dendritic overgrowths (Fig. 3b). They also contain euhedral Cr-spinel crystals.

Mesocrysts of clinopyroxene (Ø 0·1–0·5 mm) and plagioclase (Ø 0·1–0·2 mm) are exclusively observed in samples from day 5 of the eruption (Figs 3c and 4, Table 2). Clinopyroxene mesocrysts are Al-, Ti-rich and Na-, Cr-depleted salite or augite with sector-zoning ($En_{51–42}$ $Fs_{14–10}$ $Wo_{46–37}$, 2·22–6·35 wt % Al_2O_3, 0·89–2·69 wt % TiO_2, 0·00–0·43 wt % Na_2O, 0·17–0·98 wt % Cr_2O_3). Plagioclase mesocrysts have a composition in the range $An_{71–66}$. Clinopyroxene and plagioclase mesocrysts are grouped into clusters, in which plagioclase laths crosscut clinopyroxene grains. Importantly, plagioclase crystals have a well-faceted lath-like shape and are undeformed, whereas clinopyroxene grains have corroded shapes and display undulose extinction. It is also important to note that plagioclase–clinopyroxene clusters are devoid of olivine and spinel, whereas olivine ± spinel clusters are devoid of plagioclase and clinopyroxene.

Microcrysts

In the groundmass of picrobasalts and picrites the volume proportion of microcrysts relative to matrix glass increases from the chilled margins of the samples toward their interior (Fig. 3d–f). Samples quenched in water and lapilli contain a smaller fraction of microcrysts than air-cooled samples.

In the glass-poor groundmass of sample interiors, two textures of microcryst are observed: larger blocky (i.e. with a small number of faces) microcrysts (Ø 10–100 μm) of olivine + clinopyroxene + plagioclase (Fig. 3d), and tiny fibrous (i.e. with an elongated or feather-like shape) microcrysts (Ø < 10 μm) of olivine + clinopyroxene + plagioclase + Fe-Ti oxides (Fig. 3f). Fibrous textures are also observed as dendritic overgrowths on the edges of blocky olivine microcrysts (Fig. 3e). In lapilli and towards the chilled margins of the samples, tiny fibrous microcrysts and dendritic overgrowths disappear and only the population of larger blocky microcrysts remains. Fibrous microcrysts and dendritic overgrowths are therefore considered to have crystallized during sample cooling and are not considered further here. On the other hand, blocky microcrysts appear to have crystallized before quenching and hence are relevant to magmatic and/or eruptive processes.

The texture and composition of the larger blocky microcrysts is homogeneous in all of the samples, whatever their location in the sample interior or chilled margin. The composition of blocky olivine microcrysts is in the range $Fo_{83–73}$ (i.e. higher Fe contents than macrocrysts and mesocrysts), with a narrower range from Fo_{82} to Fo_{79} at their edges in contact with the matrix glass (Fig. 4, Table 2). Blocky olivine microcrysts display two special types of morphologies according to the terminology of Faure & Schiano (2004): closed hopper (Fig. 3g) and complex swallowtail shapes (Fig. 3h). The closed hopper morphology consists of an hourglass shape with pairs of funnel-shaped cavities symmetrically arranged along the [00l] axis about the centre of the crystal. The cavities are filled with melt and then closed by crystal growth, thus constituting primary melt inclusions. A single crystal may contain up to three symmetrical pairs of melt inclusions (Fig. 3g); however, one or two pairs are more commonly observed. The complex swallowtail morphology consists of interlocking closed hoppers oriented in the same direction and merged into a single crystal (Fig. 3h). The complex swallowtail crystals contain several primary melt inclusions trapped at the junction of closed hoppers or within the closed hoppers. A shrinkage bubble is occasionally found in the melt inclusions of the two crystal types. Both morphologies occasionally contain randomly

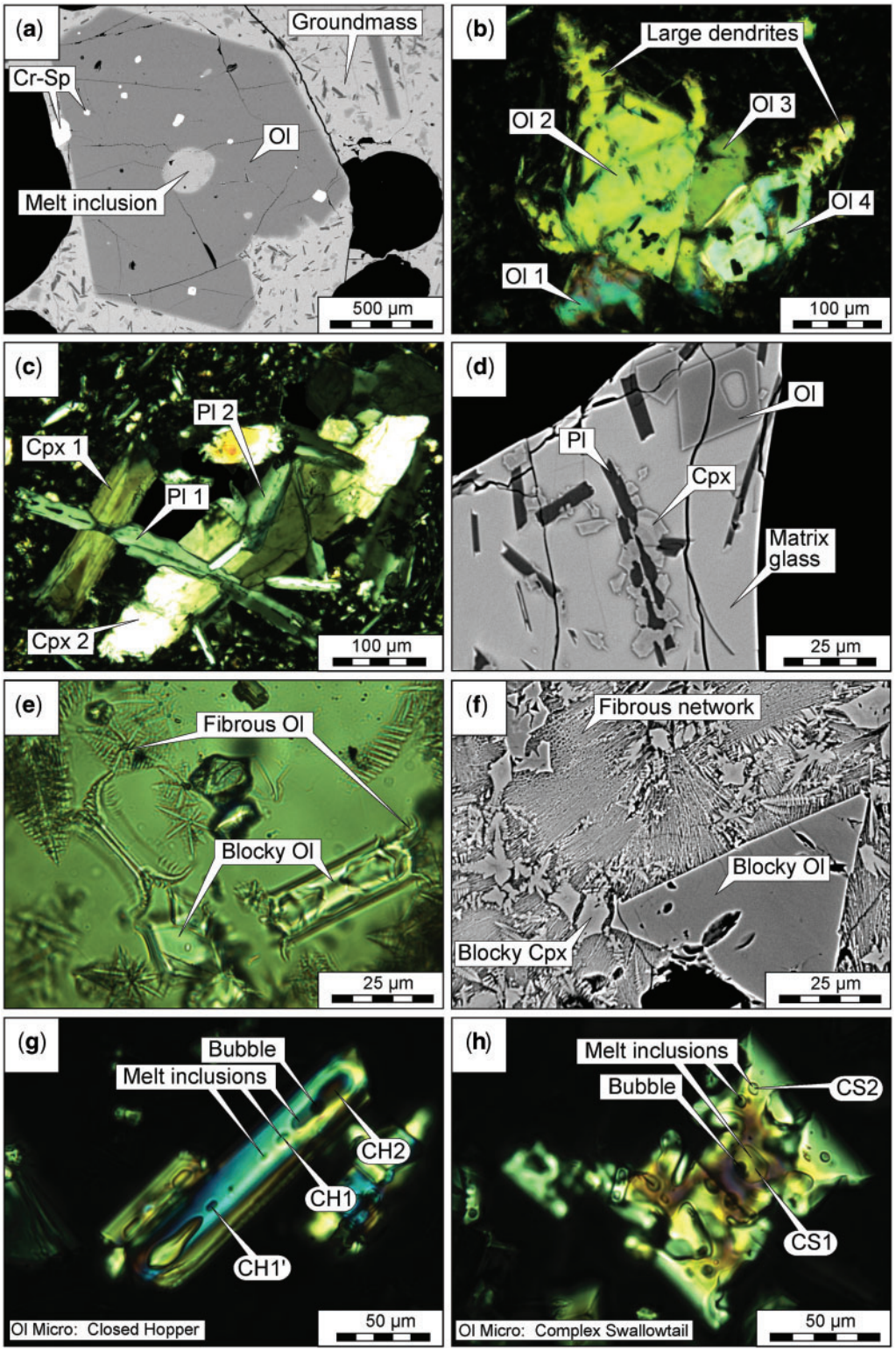

Fig. 3. Crystal populations observed in the samples of the December 2005 eruption: (a) olivine macrocryst hosting a melt inclusion and Cr-spinel microcrysts [day 24, water-quenched sample, backscattered electron (BSE) image]; (b) cluster of four olivine mesocrysts decorated with large dendrites (day 5, air-cooled sample, transmitted light photomicrograph with crossed Nicols); (c) complex clusters of intersertal clinopyroxene and plagioclase mesocrysts (day 5, air-cooled sample, transmitted light photomicrograph with crossed Nicols); (d) blocky microcrysts of Ol + Aug + Pl with dendritic overgrowths (<5 μm) in a glass-rich matrix (day 15, margin of water-quenched sample, BSE image); (e) fibrous and blocky textures of olivine microcrysts in a glass-poor groundmass (day 24, margin of water-quenched sample, transmitted light photomicrograph with plane polarization); (f) blocky microcrysts surrounded by a network of fibrous microcrysts with interstitial glass (day 24, core of water-quenched sample, BSE image); (g) closed hopper-shaped olivine microcryst with three pairs of melt inclusions symmetrical about the centre of the grain (day 24, water-quenched sample, transmitted light photomicrograph with crossed Nicols); (h) complex swallowtail-shaped olivine microcryst exhibiting melt inclusions (day 24, water-quenched sample, transmitted light photomicrograph with crossed Nicols). Mineral abbreviations are after Kretz (1983).

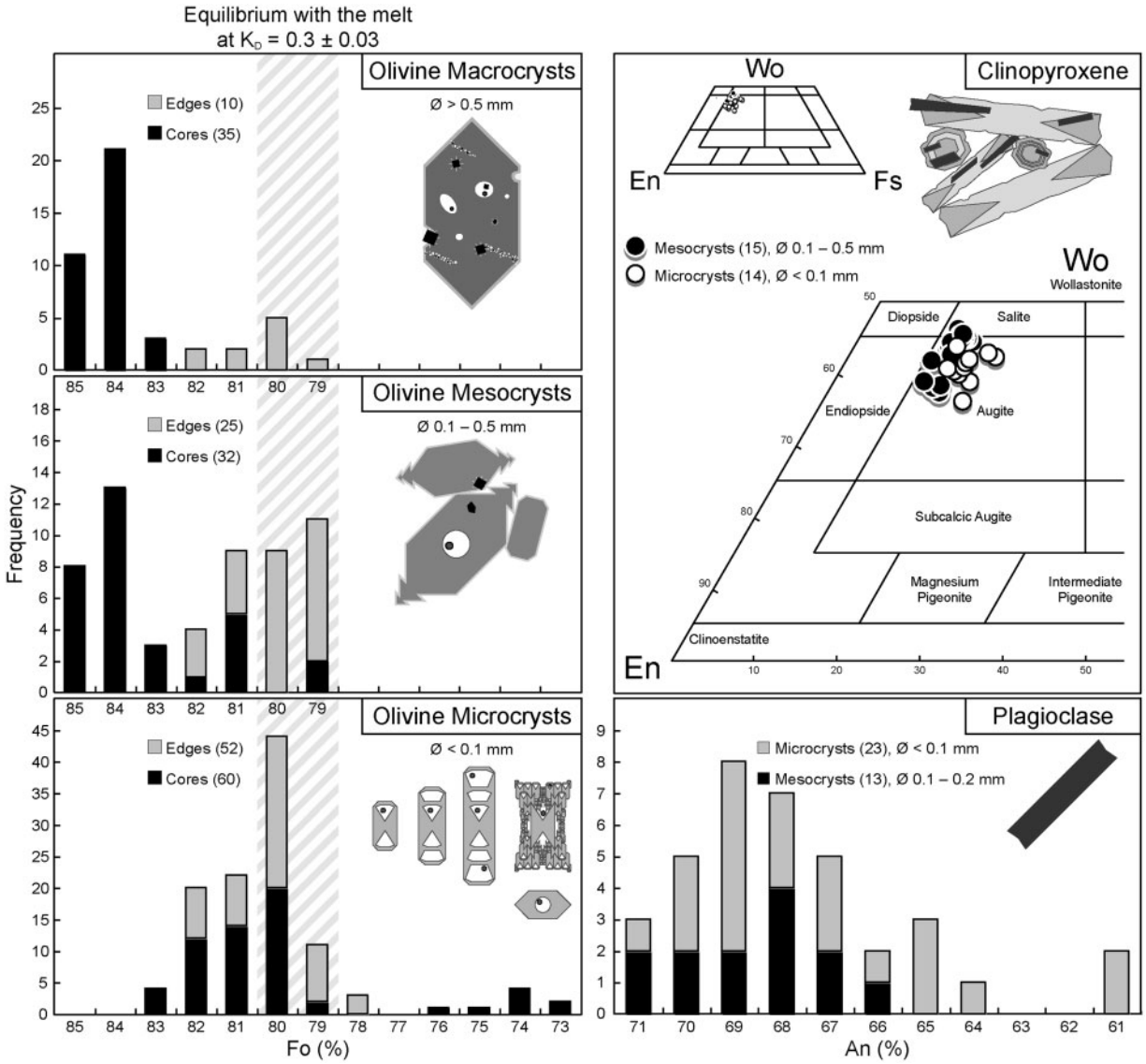

Fig. 4. Compositions and shapes of olivine, clinopyroxene and plagioclase populations observed in the samples of the December 2005 eruption.

occurring inclusions of euhedral Cr-spinel. The closed hopper morphology is more frequently observed than the complex swallowtail morphology. Blocky olivine microcrysts also display small dendritic overgrowths (<5 μm) on their edges. It should be noted that Drever & Johnston (1957) reported similar olivine morphologies in the groundmass of other picrites.

Clinopyroxene microcrysts are sector-zoned augite of composition $En_{48–40}$ $Fs_{18–12}$ $Wo_{43–36}$ (i.e. with higher Fe contents than clinopyroxene mesocrysts; Fig. 4, Table 2) with an irregular shape, and containing 2·44–7·31 wt % Al_2O_3, 1·22–3·02 wt % TiO_2, 0·12–0·47 wt % Na_2O and 0·04–0·93 wt % Cr_2O_3. Plagioclase microcrysts consist of $An_{71–61}$ laths (similar to the composition of plagioclase mesocrysts; Fig. 4, Table 2). They occur alone in the mesostasis or crosscut and embed clinopyroxene microcrysts (Fig. 3d). Both clinopyroxene and plagioclase microcrysts are aggregated, yielding clusters similar to the mesocrysts of day 5 sample.

Composition of melt inclusions and matrix glasses

The major element compositions of matrix glasses and melt inclusions in olivine microcrysts are reported in Table 3. No significant alkali loss is observed in a comparison of matrix glasses (analysed with a defocused beam) and melt inclusions (analysed with a focused beam). Within each closed hopper olivine crystal, the two melt

Table 2: *Representative analyses of the crystal populations*

	Olivine macrocryst		Olivine mesocryst		Blocky olivine microcrysts				Clinopyroxene mesocryst	Clinopyroxene microcryst	Plagioclase microcryst	Cr-spinel inclusion
Shape:	Polyhedral		Dendritic polyhedral		Closed hopper		Complex swallowtail		Anhedral	Anhedral	Lath	Euhedral
	Core	Edge	Core	Edge	Core	Edge	Core	Edge				
wt %												
SiO_2	40·08	39·38	40·36	39·30	39·66	38·66	38·18	39·40	51·26	48·39	51·27	—
Al_2O_3	—	—	—	—	—	—	—	—	2·99	6·40	30·35	17·24
FeO_t	14·58	18·48	14·85	19·1	16·17	18·65	23·88	18·38	8·13	8·64	0·99	28·16
MnO	0·22	0·26	0·24	0·16	0·13	0·34	0·29	0·31	0·20	0·21	0·07	0·45
MgO	44·86	41·37	44·84	41·11	42·69	41·56	36·89	41·31	17·4	14·52	0·19	11·96
CaO	0·27	0·35	0·23	0·47	0·40	0·44	0·43	0·51	18·71	19·16	13·98	—
Na_2O	0·02	—	—	0·04	—	0·06	0·03	—	0·19	0·29	3·28	0·06
K_2O	—	—	0·01	0·02	0·04	0·04	—	0·05	—	0·02	0·11	0·03
TiO_2	—	0·05	0·01	0·09	0·06	0·11	0·04	0·08	1·24	2·48	0·11	2·83
P_2O_5	0·13	—	0·02	0·06	0·12	0·09	—	0·04	—	0·32	0·20	—
NiO	0·24	0·10	0·32	0·09	0·18	0·25	0·11	0·03	—	0·06	0·05	0·17
Cr_2O_3	0·04	0·03	0·04	0·01	0·02	0·07	0·02	0·02	0·33	0·29	—	39·54
Total	100·43	100·01	100·92	100·45	99·55	100·25	99·88	100·13	100·44	100·78	100·59	100·42
No. O/cation	4	4	4	4	4	4	4	4	6	6	32	4
Si	1·00	1·01	1·00	1·00	1·01	0·99	1·00	1·01	1·88	1·78	9·31	—
Al	—	—	—	—	—	—	—	—	0·13	0·28	6·50	0·64
Fe	0·30	0·40	0·31	0·41	0·34	0·40	0·53	0·39	0·25	0·27	0·15	0·74
Mn	0·01	0·01	0·01	—	—	0·01	0·01	0·01	0·01	0·01	0·01	0·01
Mg	1·67	1·57	1·66	1·56	1·61	1·59	1·45	1·57	0·95	0·80	0·05	0·56
Ca	0·01	0·01	0·01	0·01	0·01	0·01	0·01	0·01	0·73	0·76	2·72	—
Na	—	—	—	—	—	—	—	—	0·01	0·02	1·16	—
K	—	—	—	—	—	—	—	—	—	—	0·03	—
Ti	—	—	—	—	—	—	—	—	0·03	0·07	0·01	0·07
P	—	—	—	—	—	—	—	—	—	0·01	0·03	—
Ni	0·01	—	0·01	—	—	—	—	—	—	—	0·01	—
Cr	—	—	—	—	—	—	—	—	0·01	0·01	—	0·98
Total	3·00	2·99	3·00	3·00	2·99	3·01	3·00	2·99	4·00	4·00	19·97	3·00
Mg-no.*	0·86	0·82	0·86	0·81	0·84	0·82	0·75	0·82	0·83	0·75	0·28	0·43
$K_{D\ Matrix}$†	0·23	0·32	0·24	0·33	0·27	0·32	0·46	0·32				
	Fo85	Fo80	Fo84	Fo79	Fo82	Fo80	Fo73	Fo80	En49	En44	An71	
									Fs13	Fs15	Ab28	
									Wo38	Wo42	Or1	

The compositions of olivine edges were obtained from spots at a distance of <10 μm from the border of crystals.
*Mg-number = atomic ratio $Mg/(Mg + Fe^{2+})$.
†Coefficient of distribution $K_{D\ \frac{Ol-Liq}{Mg-Fe}} = \left(X^{Mg}_{Liq}/X^{Mg}_{Ol}\right)/\left(X^{Fe^{2+}}_{Liq}/X^{Fe^{2+}}_{Ol}\right)$ modelled from Toplis (2005) between olivine crystals and the uniform glassy matrix (day 24 sample).

inclusions of a given symmetrical pair have a similar composition (e.g. CH1 and CH1' in Fig. 3g, Table 3). However, the composition varies from one pair of melt inclusions to the next (e.g. CH1 and CH2 in Fig. 3g, Table 3). As for most eruption products of Piton de la Fournaise, the composition of the matrix glasses is similar to the bulk-rock composition of the Steady State Basalts. The coefficient of distribution of Fe–Mg (K_D, Roedder & Emslie, 1970) between the matrix glasses and the edges of olivine macrocrysts, mesocrysts and microcrysts ($Fo_{80–79}$) is close to the equilibrium value of 0·3 ± 0·03 computed using the method of Toplis (2005). Conversely, the K_D values indicate

Table 3: *Representative analyses of glass inclusions in olivine microcrysts and matrix glasses for the December 2005 eruption*

	Glassy matrixes			Melt inclusions										
Day:	2	15	24	2		5		15		24				
				CH core	CH rim	CH core	CS core	CH core	CH rim	CH1 core	CH1′ core	CH2 rim	CS core	CS rim
wt %														
SiO_2	48·95	50·07	49·81	53·15	49·45	53·16	50·74	49·88	49·51	49·92	50·48	49·76	48·82	49·66
Al_2O_3	13·60	14·19	13·59	18·02	15·65	17·04	16·80	14·63	14·59	15·61	15·87	14·42	13·84	14·44
FeO_t	11·93	11·10	11·12	7·99	7·66	8·82	7·98	10·24	10·32	8·10	9·30	8·24	14·18	9·59
MnO	0·15	0·20	0·18	0·11	0·11	0·13	0·34	0·19	0·25	0·31	0·14	0·13	0·17	0·19
MgO	5·81	5·88	6·03	2·94	4·95	1·56	1·81	5·24	5·00	2·65	2·37	4·89	2·07	2·98
CaO	10·75	11·38	11·18	8·62	12·58	12·00	13·82	11·25	11·60	13·19	13·42	12·96	11·98	13·51
Na_2O	2·51	2·74	2·79	3·26	2·95	2·13	2·91	2·89	2·65	2·82	2·62	2·48	2·44	2·54
K_2O	0·86	0·80	0·79	0·93	0·91	0·96	0·84	0·79	0·79	0·88	0·74	0·84	0·78	0·63
TiO_2	2·90	2·91	3·06	2·19	2·64	3·34	3·44	3·07	2·94	3·44	3·44	3·19	2·88	3·26
P_2O_5	0·38	0·34	0·28	0·32	0·35	1·01	0·42	0·31	0·37	0·64	0·62	0·63	0·76	0·73
NiO	0·02	—	—	0·03	—	—	0·12	—	0·06	—	0·09	—	0·02	0·05
Cr_2O_3	—	0·03	0·02	—	0·02	0·05	0·05	0·02	—	0·03	0·02	0·03	—	—
Total	97·87	99·62	99·85	97·57	97·27	100·19	99·27	98·51	98·06	97·58	99·11	97·57	97·93	97·57
CaO/Al_2O_3	0·79	0·80	0·82	0·48	0·80	0·70	0·82	0·77	0·79	0·84	0·85	0·90	0·87	0·94
K_2O/TiO_2	0·30	0·27	0·26	0·42	0·34	0·29	0·24	0·26	0·27	0·25	0·21	0·26	0·27	0·19
Mg-no.*	0·49	0·51	0·52	0·42	0·56	0·26	0·31	0·50	0·49	0·39	0·34	0·54	0·22	0·38
$K_{D\ Matrix}$†	—	—	—	0·19	0·33	0·11	0·12	0·29	0·27	0·15	0·12	0·27	0·09	0·14
CIPW														
Qtz	—	—	—	6·47	—	12·10	3·69	0·19	0·85	3·75	4·87	2·79	3·51	4·52
Pl	45·42	47·32	45·83	59·37	51·73	52·12	55·27	49·77	48·91	52·39	51·96	47·82	46·06	48·77
Or	5·20	4·73	4·67	5·50	5·38	5·67	5·02	4·73	4·73	5·32	4·37	5·08	4·67	3·78
Di	23·25	24·92	25·84	7·40	27·19	15·99	24·12	24·32	24·81	28·84	28·10	28·81	26·23	30·88
Hy	17·47	13·72	12·79	12·68	3·59	4·25	—	12·66	12·45	0·14	1·13	6·39	9·83	2·40
Ol	0·18	1·16	1·57	—	2·38	—	—	—	—	—	—	—	—	—
Ilm	5·62	5·53	5·81	4·16	5·01	6·34	6·57	5·91	5·68	6·69	6·59	6·21	5·56	6·34
Mag	1·96	1·80	1·80	1·29	1·23	1·42	1·29	1·67	1·70	1·33	1·51	1·36	2·33	1·58
Ap	0·90	0·79	0·65	0·74	0·81	2·34	0·97	0·74	0·88	1·51	1·44	1·48	1·81	1·74
Chr	—	0·04	—	—	—	—	0·07	0·03	—	0·04	0·03	0·04	—	—

CH, closed hopper; CS, complex swallowtail.
*Atomic ratio Mg-number = $Mg/(Mg + Fe^{2+})$.
†Coefficient of distribution $K_{D\ \mathrm{Mg-Fe}}^{\mathrm{Ol-Liq}} = \left(X_{\mathrm{Liq}}^{\mathrm{Mg}}/X_{\mathrm{Ol}}^{\mathrm{Mg}}\right)/\left(X_{\mathrm{Liq}}^{\mathrm{Fe^{2+}}}/X_{\mathrm{Ol}}^{\mathrm{Fe^{2+}}}\right)$ modelled from Toplis (2005) between melt inclusions and host olivine crystals.

disequilibrium between the matrix glasses and olivine cores at $Fo_{85–81}$ and $Fo_{78–73}$ (Fig. 4). The K_D values also indicate disequilibrium between the melt inclusions and their host olivine microcrysts using the same method.

In Fig. 5, the composition of melt inclusions, matrix glasses and bulk-rocks is reported as oxide ratios of elements incompatible in olivine, to exclude artefacts in the composition of the melt inclusions caused by post-entrapment epitaxial crystallization or iron diffusion (in olivine microcrysts Al_2O_3, K_2O, TiO_2 and P_2O_5 are below the detection limit and CaO is in the range 0·24–0·46 wt %). In Fig. 5a, the matrix glasses have a narrow range of K_2O and P_2O_5 contents (0·55–0·86 and 0·27–0·38 wt %, respectively). Bulk-rock contents are similar in the samples of days 2 and 5 (picrobasalts) but lower in those of days 15 and 24 (oceanites). Melt inclusions

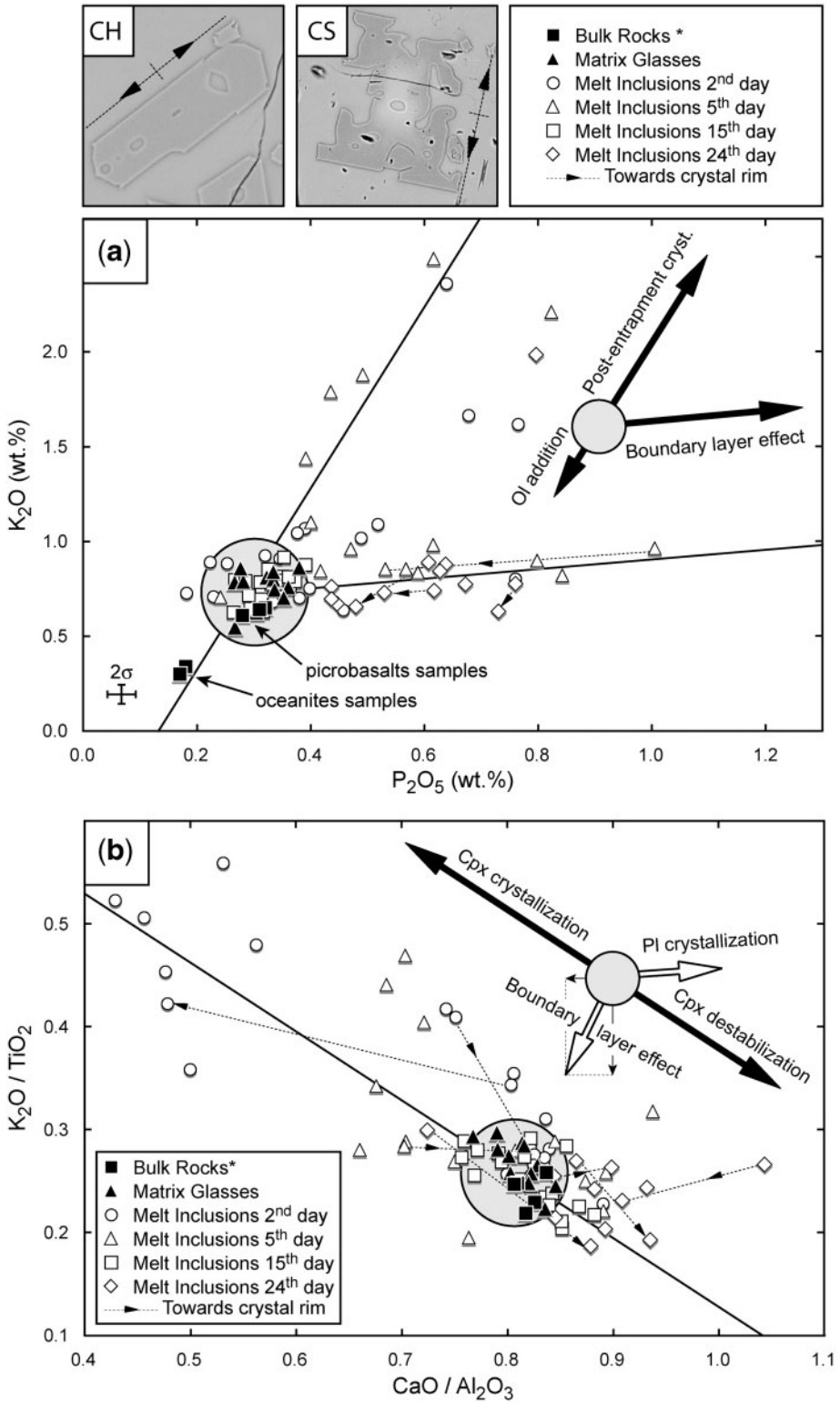

Fig. 5. (a) K_2O vs P_2O_5 contents and (b) K_2O/TiO_2 vs CaO/Al_2O_3 ratios in bulk-rocks, matrix glasses and olivine microcryst-hosted melt inclusions for the sample set of the December 2005 eruption. *Bulk rock data of Vlastélic *et al.* (2007). Error bars are smaller than the symbols in (b). CH, closed hopper-shaped olivine microcryst (50 μm long BSE image); CS, complex swallowtail-shaped olivine microcryst (50 μm long BSE image).

have compositions either similar to the matrix glasses, or specifically enriched in P_2O_5 (up to 1·01 wt %) or enriched in both oxides (up to 2·49 wt % K_2O and 0·82 wt % P_2O_5) with respect to matrix glasses. In Fig. 5b, CaO/Al_2O_3 and K_2O/TiO_2 ratios in matrix glasses are very homogeneous (0·79–0·83 and 0·25–0·30, respectively) and similar to those of the bulk-rocks. In contrast, the melt inclusions show a much wider range of CaO/Al_2O_3 and K_2O/TiO_2 ratios (0·48–1·06 and 0·19–0·54, respectively). Importantly, the CaO/Al_2O_3 and K_2O/TiO_2 ratios of the melt inclusions respectively increase and decrease in the course of the eruption whereas those of matrix glasses and bulk-rocks remain constant.

DISCUSSION

Crystal morphologies and temperature of the magma

The morphology of the crystals forming from a magma depends on variations in temperature, pressure and melt composition, and may hence be used to reconstruct the crystallization history of the magma. To do so, it is first important to assess whether these crystals developed before the eruption, in the surface lava flows or during the quench. Fibrous microcrysts and overgrown edges of larger crystals are clearly related to the quench, as they are more abundant in air-cooled samples (Fig. 3f) than in water-quenched samples, and in the interior of water-quenched samples than in their outer parts (Fig. 3d and e). This was also noted for pillow lavas by Kirkpatrick (1979) and experimentally reproduced by Faure *et al.* (2007). On the other hand, blocky microcrysts are equally abundant in water-quenched and air-cooled samples, and even occur in lapilli, showing that crystallization occurred before the magma reached the surface.

For olivine, microcryst core compositions in the ranges $Fo_{83–81}$ and $Fo_{78–73}$ are in disequilibrium with the matrix glass (Fig. 4, Table 2), indicating that the blocky microcrysts grew in the magma before it reached the surface. In contrast, their $Fo_{80–79}$ edges appear to have formed later, near the surface, in equilibrium with the matrix glass. The scattered compositions of olivine edges in the range $Fo_{82–81}$ (Fig. 4) may be partly an analytical artefact between thin crystal edges $Fo_{80–79}$ (<10 μm) and Mg-rich cores. Consequently, the morphologies of the blocky microcrysts can provide evidence of magmatic processes in the magma chamber or in the conduit.

The degree of undercooling ΔT (i.e. the temperature difference between the magma and its liquidus) has been shown to be the most important factor controlling olivine morphology (Donaldson, 1976). For example, closed hopper and complex swallowtail blocky olivine microcrysts have been recognized in basalts from the Mid-Atlantic Ridge and experimentally reproduced by applying cooling–heating cycles below the liquidus and above the solidus of a synthetic basaltic melt (Faure & Schiano, 2004). The complex swallowtail shape was obtained with large undercooling ($\Delta T = 132$°C below the liquidus, cooling rate at 1890°C/h) and subsequent heating ($\Delta T = 54$°C for 5 min). The closed hopper shape was obtained with smaller undercooling ($\Delta T = 70$°C, cooling rate at 437°C/h) and reheating ($\Delta T = 34$°C for 5 min). Importantly, one pair of melt inclusions was trapped in synthetic closed hopper crystals during each cycle of cooling and reheating. Accordingly, Faure & Schiano (2004) interpreted the shapes of microcrysts in Mid-Atlantic Ridge basalts as due to thermal convection within the axial magma chamber.

The closed hopper and complex swallowtail olivine microcrysts found in our samples (Fig. 3g and h) are similar in shape to those of the Mid-Atlantic Ridge and synthetic basalts. This suggests that the Piton de la Fournaise magmas also experienced repeated cooling–heating cycles prior to reaching the surface. Natural closed hopper crystals have trapped up to three pairs of melt inclusions (Fig. 3g) and hence must have undergone at least three cooling–heating cycles. According to MELTS modelling (Ghiorso & Sack, 1995), set at the quartz–fayalite–magnetite (QFM) buffer with an estimated composition of the parental magma at Piton de la Fournaise (Ludden, 1978; Famin *et al.*, 2009), the liquidus of olivine occurs at 1230 ± 10°C over a large range of pressures (0·1–100 MPa) and water contents (0·1–1 wt %, Fig. 6). Consequently, the undissolved shape of the olivine microcrysts implies that their temperature never exceeded 1240°C, whatever their morphologies.

The history of clinopyroxene meso- and microcrysts in the magma can also be constrained from their composition and texture. Their Ti-rich and Na-, Cr-depleted compositions suggest that clinopyroxene crystallization occurred at low pressures, possibly at less than 4 km depth (Kornprobst *et al.*, 1981; Nimis, 1999). Again using MELTS at the QFM buffer for the parental magma at 0·1–100 MPa, clinopyroxene joins the crystallizing assemblage at 1130 ± 10°C even after exsolution of water (Fig. 6). Sector-zoning and the presence of Al in the pyroxene indicate that the incorporation and distribution of elements in the mineral were controlled by interface kinetics (Lofgren *et al.*, 2006; Schwandt & McKay, 2006). The experimental data of Kouchi *et al.* (1983) have shown that clinopyroxene acquires sector-zoning during rapid growth at low degrees of undercooling ($\Delta T = 13–45$°C). In addition, the corroded shape of the clinopyroxene crystals indicates that this mineral became unstable in the magma after crystallization. Owing to the narrow range of melt compositional variations (Table 3), the destabilization of clinopyroxene was most probably controlled by temperature. The fact that temperatures up to 1170°C have been measured in

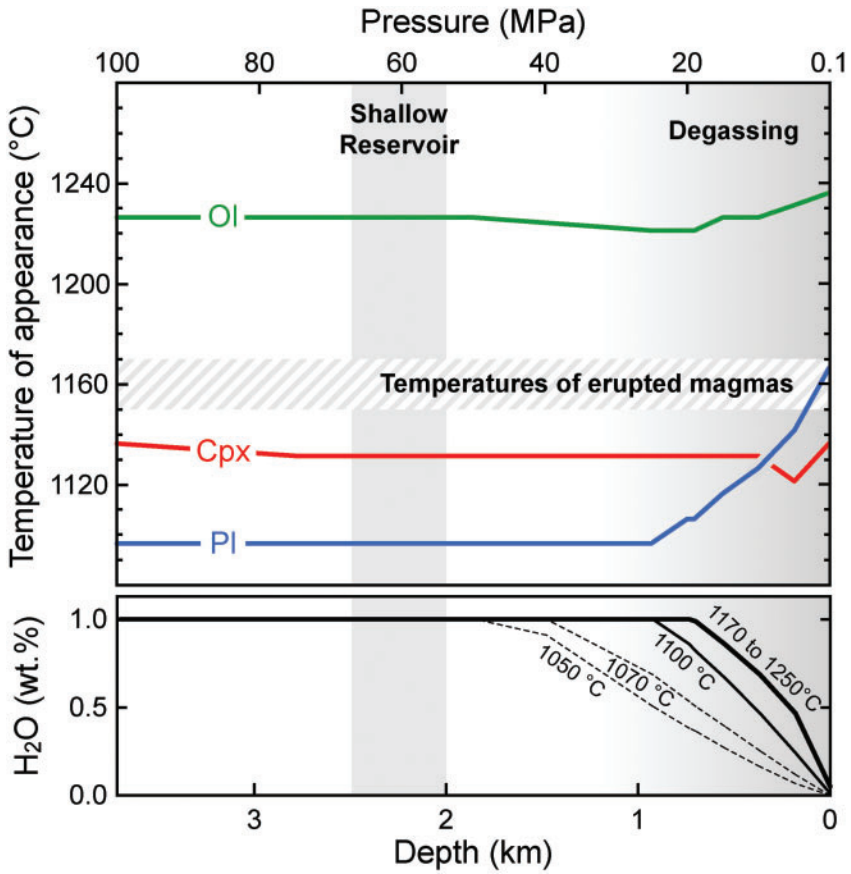

Fig. 6. Numerical simulations using MELTS (Ghiorso & Sack, 1995) for fractional crystallization from 1300 to 1050°C (5°C increment, QFM buffer) of a parental magma composition 47·7 wt % SiO_2, 2·7 wt % TiO_2, 13·25 wt % Al_2O_3, 1·6 wt % Fe_2O_3, 10·1 wt % FeO, 0·17 wt %, MnO, 9·5 wt % MgO, 0·05 wt % NiO, 10·5 wt % CaO, 2·45 wt % Na_2O, 0·67 wt % K_2O, 0·3 wt % P_2O_5, 0·1 wt % CO_2 and 1 wt % H_2O [in Famin *et al.* (2009); adapted from Ludden (1978) and Bureau *et al.* (1998)].

erupted lavas (Coppola *et al.*, 2007; Boivin & Bachèlery, 2009) suggests that the magnitude of reheating may have easily exceeded the liquidus of clinopyroxene in the crystallizing assemblage (i.e. 1130 ± 10°C). Consequently, we interpret the presence of corroded crystals of clinopyroxene as further evidence of cooling and reheating, below and above 1140°C. Possible explanations for the undulose extinction of clinopyroxene include compaction in cumulates or impacts between suspended crystals (e.g. Komar, 1972, 1976). In the former case, it is more likely that plastic deformation occurred in the cooler parts of the magma storage system, before subsequent dissolution. In the latter case, deformation may have occurred before, during and/or after reheating.

The occurrence of clinopyroxene and plagioclase in clusters and their crosscutting relationships indicate that plagioclase crystallized together with clinopyroxene (Fig. 3c and d). Given that plagioclase is prone to crystallize in the melt (~45% normative plagioclase in matrix glasses; Table 3) but reluctant to nucleate (Gibb, 1974), this mineral could have used clinopyroxene as a substrate to precipitate. In contrast to clinopyroxene, the unzoned composition and the undissolved shape of the plagioclase microcrysts indicate that these crystals did not record reheating or chemical variations in the liquid. Rather, their lath-like shape (Fig. 3c and d) suggests slow growth at a low degree of undercooling ($\Delta T < 40$°C in the anhydrous experiments of Kirkpatrick *et al.*, 1979). According to our MELTS simulations, plagioclase crystallizes below 1100°C with 1 wt % H_2O in the melt (the maximum H_2O content in melt inclusions; Bureau *et al.*, 1998), and below 1180°C if the water content was less than 0·1 wt % (Fig. 6). Because the erupted magmas have temperatures up to 1170°C (Coppola *et al.*, 2007; Boivin & Bachèlery, 2009), the exsolution of water probably enhanced plagioclase crystallization.

Causes of compositional variations in melt inclusions

The compositional variations in olivine microcryst-hosted melt inclusions imply that the olivine crystals sampled different magma compositions during crystallization

(Table 3, Fig. 5). An external cause of magma heterogeneity, such as re-feeding or contamination of the plumbing system, is unlikely because the matrix glasses have a uniform composition [bulk compositional variations are only due to olivine addition from picrobasalts (days 2 and 5) to picrites (days 15 and 24)]. Famin *et al.* (2009) also noted that contamination, if it does occur, does not involve significant volumes of contaminants that could change the major element concentrations. In addition, Pb isotope data do not show any evidence for refilling or contamination during the December 2005 eruption (Vlastélic *et al.*, 2007).

Those melt inclusions showing simultaneous enrichment in K_2O and P_2O_5 (Fig. 5a), probably experienced post-entrapment crystallization, as olivine simultaneously rejects K and P. This process was apparently stronger in the small melt inclusions ($Ø < 10\,\mu m$) in the air-cooled samples, probably because of intense epitaxial overgrowth on the inclusion walls. In contrast, post-entrapment crystallization cannot explain the specific enrichment in P_2O_5 in the other melt inclusions. Element diffusion has to be examined because it can modify the composition of the melt around rapidly growing olivine crystals (Faure & Schiano, 2005). Given that P diffuses more slowly than K in the melt (Jambon, 1982; Harrison & Watson, 1984), this element may accumulate at the contact with olivine and form a boundary layer enriched in P_2O_5. Subsequent olivine growth may embay portions of such boundary layers and seal them off from the magma, yielding melt inclusions enriched in P_2O_5. The fact that the P_2O_5 contents decrease from one melt inclusion to the next within a single crystal (Fig. 5a) suggests that such boundary layers were transient before sealing. Melt inclusions that record boundary layer effects can also experience post-entrapment crystallization. They are expected to have higher K_2O contents than the matrix glass, which may correspond to an average of melt inclusions with scattered compositions.

The co-variations of CaO/Al_2O_3 and K_2O/TiO_2 ratios in the melt inclusions (Fig. 5b) have also to be considered in the context of compositional effects in the olivine boundary layer. In the melt, Ca diffuses faster than Al (Liang *et al.*, 1996) and K diffuses faster than Ti (Jambon, 1982; LaTourrette *et al.*, 1996). Fast crystallization of olivine is therefore expected to enrich the melt inclusions in Al and Ti, yielding low CaO/Al_2O_3 and low K_2O/TiO_2 ratios. However, these ratios show opposite variations in the melt inclusions from this study, indicating that diffusion kinetics is not the main cause of chemical variations in the trapped melts. These variations are neither controlled by olivine nor spinel equilibrium crystallization–dissolution, because these minerals cannot yield opposite CaO/Al_2O_3 and K_2O/TiO_2 variations given their composition (Table 3). In contrast, clinopyroxene and plagioclase may control these two ratios. The crystallization of clinopyroxene consumes Ca and Ti, which lowers the CaO/Al_2O_3 ratio and increases the K_2O/TiO_2 ratio in the melt. Conversely, the effect of clinopyroxene dissolution is to release Ca and Ti in the melt, increasing the CaO/Al_2O_3 ratio and decreasing the K_2O/TiO_2 ratio. Plagioclase crystallization has the opposite effect because it increases the CaO/Al_2O_3 ratio and decreases the K_2O/TiO_2 ratio in the melt. The reverse is obtained with plagioclase dissolution. In the CaO/Al_2O_3 vs K_2O/TiO_2 diagram (Fig. 5b), the melt inclusion data from this study yield a slope of −0·5 consistent with the crystallization or destabilization of pure clinopyroxene without significant influence of plagioclase. This is in agreement with the suggestion of Albarède *et al.* (1997) that plagioclase fractionation is negligible in the Steady State Basalts. We therefore suggest that the co-variation of CaO/Al_2O_3 and K_2O/TiO_2 in the melt inclusions results from clinopyroxene crystallization and dissolution (Fig. 5b). The growth mode of closed hopper and complex swallowtail shaped olivine implies that their hosted melt inclusions were trapped during reheating and simultaneously with clinopyroxene crystallization or dissolution. This means that clinopyroxene did not dissolve immediately during reheating but may have co-crystallized with olivine. This can be explained if olivine and clinopyroxene microcrysts are both metastable, having rapidly grown in a cooler magma. Indeed, their crystallization was probably not completed during cooling and could have continued during a reheating event by switching the growth mechanism from diffusion-controlled to interface-controlled (Faure & Schiano, 2004). Olivine and clinopyroxene may co-crystallize during reheating but at a lower growth rate and at temperatures below 1140°C. At higher temperatures, clinopyroxene will dissolve. In contrast, the high liquidus temperature of olivine (1230°C) allowed this mineral to continue to crystallize and to seal the melt inclusions. Consequently, we interpret the compositions of olivine-hosted melt inclusions as further evidence of temperature cycling in the magma, together with the corroded texture of clinopyroxene meso- and microcrysts. The temperature of the magma must oscillate below and above the liquidus of clinopyroxene (1140°C). The fact that plagioclase is not involved in the compositional variations of the melt suggests that this mineral crystallizes after the cooling–heating cycles recorded by olivine, clinopyroxene and melt inclusions.

Magma dynamics in a hotspot volcano

There are two possible explanations for the observed changes in composition and texture of the microcrysts. A first scenario could be refilling of magma in the plumbing system; however, this seems unlikely because the melt has an almost steady-state major element and Pb isotope composition throughout the 2005 eruption and the hosted olivine macrocrysts have a shallow origin (Vlastélic *et al.*,

2007; Famin *et al.*, 2009). In addition, the seismic activity during December 2005 does not support refilling, as it was restricted to a depth shallower than 2·5 km below the surface (Peltier *et al.*, 2008) whereas it went much deeper during the 1998 refilling event (Battaglia *et al.*, 2005*b*). Moreover, recharge with a hotter magma cannot explain the multiple cooling–heating cycles recorded by the olivine microcrysts (Fig. 3g). These thermal variations are neither indicative of water exsolution nor polybaric crystallization given that the liquidus temperature of olivine and clinopyroxene is almost constant from 100 to 0·1 MPa (Fig. 6).

A second, more probable, explanation is that the olivine and clinopyroxene blocky microcrysts have travelled through a thermally and compositionally heterogeneous magma chamber (Fig. 7). We suggest that their cyclic transport is caused by thermal and/or compositional convection in the shallow magma reservoir below the Piton de la Fournaise volcano. In cooler zones (i.e. below 1140°C), presumably on the margins of the chamber, clinopyroxene crystallizes together with olivine, which traps a Ca- and Ti-depleted magma (Fig. 7a). Some of the crystals are then transported to hotter and probably inner zones (above 1140°C and below 1230°C), in which clinopyroxene crystals are destabilized and olivine microcrysts trap Ca- and Ti-enriched melt inclusions. It is noteworthy that Ca- and Ti-poor melt inclusions are more abundant at the beginning of the eruption whereas Ca- and Ti-rich melt inclusions become more abundant in olivine microcrysts toward the end of the eruption. This may suggest that the cyclic transport of fresh hot magma towards the cold margins gradually extracted and dissolved clinopyroxene from the chamber's walls, yielding progressive Ca- and Ti-enrichment of the melt in this zone. The matrix glass of the lavas does not evolve with time, probably because a large part of the chamber is chemically well mixed by convection, except at the margins.

On the other hand, plagioclase has only limited influence in the reservoir. Plagioclase microcrysts do not record cooling–heating cycles and evidence of feldspar fractionation is absent both in the melt inclusions (Fig. 5b) and the magmas (Albarède *et al.*, 1997). However, the occurrence of plagioclase and clinopyroxene clusters indicates that a small amount of plagioclase co-crystallized with clinopyroxene in the cooler margins of the chamber. The fact that clustered plagioclase shows no evidence of dissolution after transport in hotter magma may be explained if the dissolution rate of plagioclase is lower than that of clinopyroxene. This may suggest that the dissolution kinetics of plagioclase is controlled by the slow diffusion of constituents such as Al at the crystal–melt interface (e.g. Donaldson, 1985, 1990). The high normative plagioclase contents of the matrix glasses (~45%, Table 3) could also indicate that the melt is supersaturated with plagioclase and cannot contain more dissolved components of this mineral at magmatic temperatures. Another possibility is that the partial dissolution of clinopyroxene increased locally the stability of adjacent plagioclase by releasing feldspar constituents such as Ca and Al (Table 2). Conversely, non-clustered plagioclase microcrysts may have a different origin. Plagioclase crystallization is favoured by water exsolution (Lipman & Banks, 1987; Hammer, 2006), and the magma drops from ~1 wt % H_2O in the chamber (according to olivine macrocryst-hosted melt inclusions) to less than 0·1 wt % H_2O in the matrix glass of the erupted lavas (Bureau *et al.*, 1998; Famin *et al.*, 2009). Non-clustered plagioclase microcrysts may therefore crystallize as a result of decompression of the magma in the conduit after leaving the reservoir and before reaching the surface (Figs 6 and 7b). Their growth rates can be estimated on the basis of magma ascent in 2–7 h, consistent with ascent rates of 0·2–2 m/s for preceding eruptions (Toutain *et al.*, 1992; Battaglia & Bachèlery, 2003; Peltier *et al.*, 2005, 2007) and exsolution of water in the last 0·2–1 km from the surface (Fig. 6, Bureau *et al.*, 1998). The resultant growth rate ranges from 10^{-6} to 10^{-9} m/s, which is a slow growth rate for plagioclase, consistent with the lath shape of the microcrysts (Kirkpatrick, 1976; Kirkpatrick *et al.*, 1979). The fact that olivine-hosted melt inclusions do not record the crystallization of plagioclase in the conduit may indicate that convection in the magma did not persist during its ascent.

One implication of our results is that convective transport of crystals through a heterogeneous magma reservoir may explain some of the chemical variations in melt inclusions. In addition to kinetic effects during crystallization (Faure & Schiano, 2005) and post-entrapment *in situ* differentiation processes (Danyushevsky *et al.*, 2000), thermal convection should be taken into account as a potential cause of compositional variability in melt inclusions.

Whether convection at Piton de la Fournaise is a transient or long-lasting process can also be evaluated on the basis of our results. At a growth rate of 10^{-6} to 10^{-10} m/s (Jambon *et al.*, 1992), the blocky olivine microcrysts would crystallize in the magma within a few days at most (1–14 h to a maximum of 6 days); that is, during or just before the eruption. The convection recorded by the olivine microcrysts is, therefore, a phenomenon contemporaneous with the transfer of magma towards surface. This short time interval implies that microcryst-hosted melt inclusions can provide instantaneous snapshots of magma convection. Throughout the December 2005 eruption, the gradual CaO/Al_2O_3 increase and K_2O/TiO_2 decrease in olivine microcryst-hosted melt inclusions (Fig. 5) suggests that destabilization of clinopyroxene is syn-eruptive. This is consistent with the progressive CaO/Al_2O_3 increase reported by Vlastélic *et al.* (2007) in the bulk lavas over the period 1998–2006 (Fig. 1) and with the assumption that the magmas remove clinopyroxene from the chamber

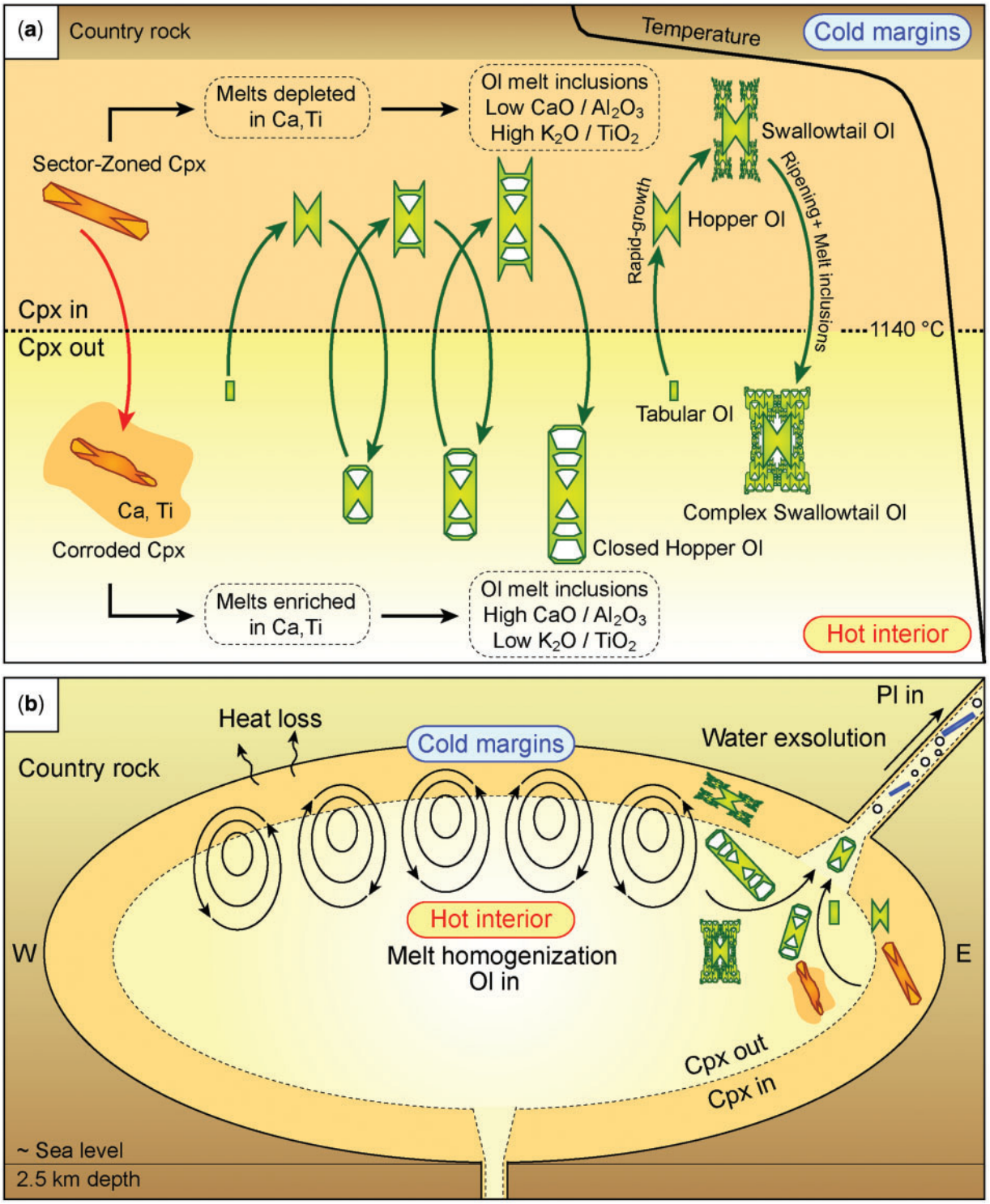

Fig. 7. (a) Temperature history of clinopyroxene and olivine microcrysts from the December 2005 eruption at Piton de la Fournaise. Corroded crystals of clinopyroxene indicate reheating above the clinopyroxene liquidus (1140°C). Olivine shapes indicate repeated cooling–heating cycles. In each closed hopper-shaped olivine, a pair of melt inclusions is trapped during each cycle. Up to three pairs of melt inclusions are observed in the olivine microcrysts. In the clinopyroxene-in zone, melt inclusions are depleted in Ca and Ti, and enriched in these elements in the clinopyroxene-out zone. In the course of the eruption, Ca and Ti concentrations increased in the melt inclusions with continuing clinopyroxene extraction and destabilization. (b) Interpretative sketch of magma dynamics during the December 2005 eruption in the shallow reservoir of Piton de la Fournaise. Olivine and clinopyroxene ± plagioclase microcrysts crystallize mostly at the cooler top margin of the chamber, and are then transported by convection to the hotter and more homogeneous interior, in which clinopyroxene is destabilized whereas olivine continues to grow. Given the small size of the microcrysts, the convection cells are probably small-scale and short-lived, suggesting a low Rayleigh number barely above the critical value. The dyke involved in the December 2005 eruption is rooted on the eastern side of the chamber. Plagioclase microcrysts crystallize in the conduit during the ascent of the magma. Arbitrary scale.

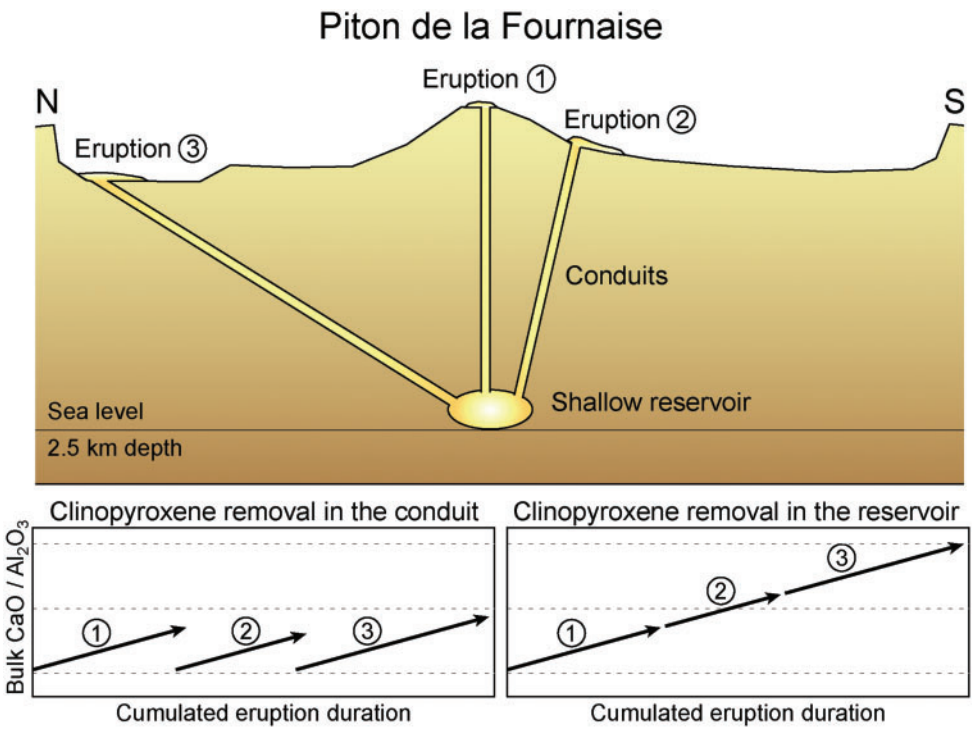

Fig. 8. Trends of magma enrichment depending on whether it occurs in the conduit or in the reservoir. In the case of clinopyroxene removal in the conduit, the CaO/Al_2O_3 increase is disrupted from one eruption to the next because of variations in the magma path. This trend is inconsistent with the continuous trend observed in the lavas (Fig. 1). In the case of syn-eruptive clinopyroxene removal in the reservoir, the CaO/Al_2O_3 increase is maintained from one eruption to the next and is similar to the trend observed in lavas. Arbitrary scale.

walls during eruptions. This process is unlikely to occur in the conduit because magmas cannot have progressively increasing CaO/Al_2O_3 bulk ratios if their path to the surface varies from one eruption to the next (Figs 2 and 8). Magmas can maintain their CaO/Al_2O_3 bulk-rock ratios only by removing clinopyroxene from a single igneous body, presumably the shallow reservoir. The small variations in the CaO/Al_2O_3 trend of the bulk lavas could suggest refilling events or variations in the rate of clinopyroxene extraction from the chamber walls. Systematic syn-eruptive Ca enrichment suggests that clinopyroxene crystals are removed from the chamber margins by convection during eruptions and not between, probably because the magma is stagnant. Convective instability would begin with the sinking of clinopyroxene and olivine crystals grown in the boundary layer at the top of the chamber, possibly leading to an eruption. This step of margin destabilization could correspond to the swarms of earthquakes recorded at the roof of the chamber just before and at the beginning of the eruptions (Nercessian *et al.*, 1996; Peltier *et al.*, 2008). For example, Harris *et al.* (2005) and Jones *et al.* (2006) have shown that the cracking of crusts and bursting of bubbles at the convective surface of Erta Ale's lava lake generates cycles of seismic wavefields. Similar disruption can occur at the top of the chamber during magma overturn involving gas and solids. If so, the rate of solidification at the upper boundary layer might be an important factor controlling the frequency of eruptions.

Convection seems to be limited to short time intervals at Piton de la Fournaise, thus favouring the interpretation of transient convection cells triggered by the thickness of the cooled margins of the chamber. The magma reservoir is more probably characterized by low Rayleigh numbers, which only episodically exceed the critical value for convection, rather than by large Rayleigh numbers ($>10^4$) and vigorous convection. Further investigation of olivine shapes in lavas from other volcanoes is necessary to assess whether transient convection is the rule or an exception in magma chambers.

CONCLUSIONS

The groundmass of the December 2005 picrite eruption at Piton de la Fournaise volcano contains olivine, clinopyroxene and plagioclase microcrysts that can be used to reconstruct the thermal history of the magma prior to reaching the surface. Olivine microcrysts show textural evidence for successive cooling and heating cycles. Corroded textures indicate that clinopyroxene crystals also underwent reheating above the liquidus of clinopyroxene after

crystallization. This partial dissolution is matched by the composition of melt inclusions in olivine microcrysts. We suggest that the cyclic temperature variations experienced by olivine and clinopyroxene microcrysts are due to thermal convection in the shallow storage zone (2–2·5 km) beneath Piton de la Fournaise. Plagioclase microcrysts crystallize in the conduit during the ascent of the magma, and do not record convection. Given the small size of the olivine microcrysts and the survival of clinopyroxene crystals, it is likely that the onset of convection preceded the December 2005 eruption by only a few days at most. These results favour models of transient, small-scale convection cells rather than more vigorous and continuous convection.

ACKNOWLEDGEMENTS

We benefited from the helpful comments of Julia Hammer, Dougal Jerram and an anonymous reviewer on an early version of the manuscript. We are also grateful to Valérie Ferrazzini and OVPF staff for discussions and some of the samples. Sandrine Mathieu and Johann Ravaux are thanked for assistance with the electron probe microanalyzer. FSE, Région Réunion and ANR MIME are the sponsors of this work. This is IPG Contribution No. 2568 and CRPG No. 2027.

REFERENCES

Aki, K. & Ferrazzini, V. (2000). Seismic monitoring and modeling of an active volcano for prediction. *Journal of Geophysical Research* **105**, 16617–16640.

Albarède, F. & Tamagnan, V. (1988). Modelling the recent geochemical evolution of the Piton de la Fournaise volcano, Réunion Island, 1931–1986. *Journal of Petrology* **29**, 997–1030.

Albarède, F., Luais, B., Fitton, G., Semet, M., Kaminski, E., Upton, B. G., Bachèlery, P. & Cheminée, J.-L. (1997). The geochemical regimes of Piton de la Fournaise volcano (Réunion) during the last 530 000 years. *Journal of Petrology* **38**, 171–201.

Allard, P. (1997). Endogenous magma degassing and storage at Mount Etna. *Geophysical Research Letters* **24**, 2219–2222.

Battaglia, J. & Bachelèry, P. (2003). Dynamic dyke propagation deduced from tilt variations preceding the March 9, 1998, eruption of the Piton de la Fournaise volcano. *Journal of Volcanology and Geothermal Research* **120**, 289–310.

Battaglia, J., Aki, K. & Ferrazzini, V. (2005*a*). Location of tremor sources and estimation of lava output using tremor source amplitude on the Piton de la Fournaise volcano: 1. *Location of tremor sources.* Journal of Volcanology and Geothermal Research **147**, 268–290.

Battaglia, J., Ferrazzini, V., Staudacher, T., Aki, K. & Cheminée, J.-L. (2005*b*). Pre-eruptive migration of earthquakes at the Piton de la Fournaise volcano (Réunion Island). *Geophysical Journal International* **161**, 549–558.

Boivin, P. & Bachèlery, P. (2009). Petrology of 1977 to 1998 eruptions of Piton de la Fournaise, La Réunion Island. *Journal of Volcanology and Geothermal Research* **184**, 109–125.

Bureau, H., Pineau, F., Métrich, N., Semet, M. P. & Javoy, M. (1998). A melt and fluid inclusion study of the gas phase at Piton de la Fournaise volcano (Réunion Island). *Chemical Geology* **147**, 115–130.

Bureau, H., Métrich, N., Semet, M. P. & Staudacher, T. (1999). Fluid–magma decoupling in a hot-spot volcano. *Geophysical Research Letters* **26**, 3501–3504.

Cayol, V. & Cornet, F. H. (1998). Three-dimensional modelling of the 1983–1984 eruption at Piton de la Fournaise Volcano, Réunion Island. *Journal of Geophysical Research* **103**, 18025–18037.

Clochiatti, R., Havette, A. & Nativel, P. (1979). Relations petrogénétiques entre les basaltes transitionnels et les océanites du Piton de la Fournaise (île de la Réunion, Océan Indien) à partir de la composition chimique des inclusions vitreuses des olivines et des spinelles. *Bulletin of Mineralogy* **102**, 512–525.

Coppola, D., Staudacher, T. & Cigolini, C. (2007). Field thermal monitoring during the August 2003 eruption at Piton de la Fournaise (La Réunion). *Journal of Geophysical Research* **112**, 1–15.

Coppola, D., Piscopo, D., Staudacher, T. & Cigolini, C. (2009). Lava discharge rate and effusive pattern at Piton de la Fournaise from MODIS data. *Journal of Volcanology and Geothermal Research* **184**, 174–192.

Danyushevsky, L. V., Della-Pasqua, F. N. & Sokolov, S. (2000). Re-equilibration of melt inclusions trapped by magnesian olivine phenocrysts from subduction-related magmas: petrological implications. *Contributions to Mineralogy and Petrology* **138**, 68–83.

Deniel, C., Kieffer, G. & Lecointre, J. (1992). New ^{230}Th–^{238}U and ^{14}C age determinations from Piton des Neiges volcano, Réunion—A revised chronology for the differentiated series. *Journal of Volcanology and Geothermal Research* **51**, 253–267.

Donaldson, C. H. (1976). An experimental investigation of olivine morphology. *Contributions to Mineralogy and Petrology* **57**, 187–213.

Donaldson, C. H. (1985). The rates of dissolution of olivine, plagioclase, and quartz in a basalt melt. *Mineralogical Magazine* **49**, 683–693.

Donaldson, C. H. (1990). Forsterite dissolution in superheated basaltic, andesitic and rhyolitic melts. *Mineralogical Magazine* **54**, 67– 74.

Drever, H. I. & Johnston, R. (1957). Crystal growth of forsteritic olivine in magmas and melts. *Transactions of the Royal Society of Edinburgh* **58**, 289–315.

Famin, V., Welsch, B., Okumura, S., Bachèlery, P. & Nakashima, S. (2009). Three differentiation stages of a single magma at Piton de la Fournaise volcano (Réunion hotspot). *Geochemistry Geophysics, Geosystems* **10**, 1–18.

Faure, F. & Schiano, P. (2004). Crystal morphologies in pillow basalts: Implications for mid-ocean ridge processes. *Earth and Planetary Science Letters* **220**, 331–344.

Faure, F. & Schiano, P. (2005). Experimental investigation of equilibration conditions during forsterite growth and melt inclusion formation. *Earth and Planetary Science Letters* **236**, 882–898.

Faure, F., Trolliard, G., Nicollet, C. & Montel, J.-M. (2003*a*). A developmental model of olivine morphology as a function of the cooling rate and the degree of undercooling. *Contributions to Mineralogy and Petrology* **145**, 251–263.

Faure, F., Trolliard, G. & Soulestin, B. (2003*b*). TEM investigation of forsterite dendrites. *American Mineralogist* **88**, 1241–1250.

Faure, F., Schiano, P., Trolliard, G., Nicollet, C. & Soulestin, B. (2007). Textural evolution of polyhedral olivine experiencing rapid cooling rates. *Contributions to Mineralogy and Petrology* **153**, 405–416.

Fukushima, Y., Cayol, V. & Durand, P. (2005). Finding realistic dike models from interferometric synthetic aperture radar data: The February 2000 eruption at Piton de la Fournaise. *Journal of Geophysical Research* **110**, 1–15.

Ghiorso, M. S. & Sack, R. O. (1995). Chemical mass transfer in magmatic processes IV. A revised and internally consistent thermodynamic model for the interpolation and extrapolation of

liquid–solid equilibria in magmatic systems at elevated temperatures and pressures. *Contributions to Mineralogy and Petrology* **119**, 197–212.

Gibb, F. G. F. (1974). Supercooling and the crystallization of plagioclase from a basaltic magma. *Mineralogical Magazine* **39**, 641–653.

Gillot, P.-Y. & Nativel, P. (1989). Eruptive history of the Piton de la Fournaise volcano, Réunion Island, Indian Ocean. *Journal of Volcanology and Geothermal Research* **36**, 53–65.

Guilbaud, M. N., Blake, S., Thordarson, T. & Self, S. (2007). Role of syn-eruptive cooling and degassing on textures of lavas from the AD 1783–1784 Laki eruption, South Iceland. *Journal of Petrology* **48**, 1265–1294.

Hammer, J. E. (2006). Volcanoes: Interpreting inclusive evidence. *Nature* **439**, 26–27.

Harris, A. J. L., Carniel, R. & Jones, J. (2005). Identification of variable convective regimes at Erta Ale Lava Lake. *Journal of Volcanology and Geothermal Research* **142**, 207–223.

Harrison, T. M. & Watson, E. B. (1984). The behavior of apatite during crustal anatexis: Equilibrium and kinetic considerations. *Geochimica et Cosmochimica Acta* **48**, 1467–1477.

Jambon, A. (1982). Tracer diffusion in granitic melt: experimental results for Na, K, Rb, Cs, Ca, Sr, Ba, Ce, Eu to 1300°C and a model of calculation. *Journal of Geophysical Research* **87**, 10797–10810.

Jambon, A., Lussiez, P. & Clocchiatti, R. (1992). Olivine growth rates in a tholeiitic basalt: An experimental study of melt inclusions in plagioclase. *Chemical Geology* **96**, 277–287.

Jaupart, C. & Parsons, B. (1985). Convective instabilities in a variable viscosity fluid cooled from above. *Physics of the Earth and Planetary Interiors* **39**, 14–32.

Jones, J., Carniel, R., Harris, A. J. L. & Malone, S. (2006). Seismic characteristics of variable convection at Erta Ale lava lake, Ethiopia. *Journal of Volcanology and Geothermal Research* **153**, 64–79.

Kazahaya, K., Shinohara, H. & Saito, G. (1994). Excessive degassing of Izu-Oshima volcano: Magma convection in a conduit. *Bulletin of Volcanology* **56**, 207–216.

Kirkpatrick, R. J. (1976). Kinetics of crystal growth from silicate melts: Anorthite and diopside. *Journal of Geophysical Research* **81**, 5715–5720.

Kirkpatrick, R. J. (1979). Processes of crystallization in basaltic pillows, Hole 396B, DSDP Leg 46. In: Heirtzler, J. R. & Dmitriev, L. *et al.* (eds) *Initial Reports of the Deep Sea Drilling Project, 46.* Washington, DC: US Government Printing Office, pp. 271–282.

Kirkpatrick, R. J., Klein, L., Uhlmann, D. R. & Hays, J. F. (1979). Rates and processes of crystal growth in the system anorthite–albite. *Journal of Geophysical Research* **84**, 3671–3676.

Komar, P. D. (1972). Mechanical interactions of phenocrysts and flow differentiation of igneous dikes and sills. *Geological Society of America Bulletin* **83**, 973–988.

Komar, P. D. (1976). Phenocrysts interactions and the velocity profile of magma flowing through dikes and sills. *Geological Society of America Bulletin* **87**, 1336–1342.

Kornprobst, J., Ohnenstetter, D. & Ohnenstetter, M. (1981). Na and Cr contents in clinopyroxenes from peridotites: a possible discriminant between 'sub-continental' and 'sub-oceanic' mantle. *Earth and Planetary Science Letters* **53**, 241–254.

Kouchi, A., Sugawara, Y., Kashima, K. & Sunagawa, I. (1983). Laboratory growth of sector zoned clinopyroxenes in the system $CaMgSi_2O_6$–$CaTiAl_2O_6$. *Contributions to Mineralogy and Petrology* **83**, 177–184.

Kretz, R. (1983). Symbols for rock-forming minerals. *American Mineralogist* **68**, 277–279.

Kushiro, I. (1978). Viscosity and structural changes of albite ($NaAlSi_3O_8$) melt at high pressures. *Earth and Planetary Science Letters* **41**, 87–90.

Lacroix, A. (1923). Minéralogie de Madagascar. In: Challamel (ed.) Paris, pp. 228.

LaTourrette, T., Wasserburg, G. J. & Fahey, A. J. (1996). Self diffusion of Mg, Ca, Ba, Nd, Yb, Ti, Zr, and U in haplobasaltic melt. *Geochimica et Cosmochimica Acta* **60**, 1329–1340.

Le Bas, M. J. (2000). IUGS reclassification of the high-Mg and picritic volcanic rocks. *Journal of Petrology* **41**, 1467–1470.

Lénat, J.-F. & Bachèlery, P. (1990). Structure and dynamics of the central zone of Piton de la Fournaise volcano. In: Lénat, J.-F. (ed.) *Le Volcanisme de la Réunion, Monographie*. Cent. De Rech. Volcanol.: Clermont-Ferrand, France, pp. 257–296.

Letourneur, L., Peltier, A., Staudacher, T. & Gudmundsson, A. (2008). The effects of rock heterogeneities on dyke paths and asymmetric ground deformation: The example of Piton de la Fournaise (Réunion Island). *Journal of Volcanology and Geothermal Research* **173**, 289–302.

Liang, Y., Richter, F. M. & Watson, E. B. (1996). Diffusion in silicate melts: II. *Multicomponent diffusion in CaO–Al_2O_3–SiO_2 at 1500°C and 1 GPa*. Geochimica et Cosmochimica Acta **60**, 5021–5035.

Lipman, P. W. & Banks, N. G. (1987). Aa flow dynamics, Mauna Loa. *US Geological Survey Professional Papers* **1350**, 1527–1567.

Lofgren, G. E., Huss, G. R. & Wasserburg, G. J. (2006). An experimental study of trace-element partitioning between Ti–Al-clinopyroxene and melt: Equilibrium and kinetic effects including sector zoning. *American Mineralogist* **91**, 1596–1606.

Ludden, J. N. (1978). Magmatic evolution of the basaltic shield volcanoes of Reunion Island. *Journal of Volcanology and Geothermal Research* **4**, 171–198.

Marsh, B. D. (1989). On convective style and vigor in sheet-like magma chambers. *Journal of Petrology* **30**, 479–530.

Martel, C., Radadi Ali, A., Poussineau, S., Gourgaud, A. & Pichavant, M. (2006). Basalt-inherited microlites in silic magmas: Evidence from Mount Pelée (Martinique, French West Indies). *Geology* **34**, 905–908.

McDougall, I. (1971). The geochronology and evolution of the young volcanic Island of Réunion, Indian Ocean. *Geochimica et Cosmochimica Acta* **35**, 261–288.

Michon, L., Saint-Ange, F., Bachèlery, P., Villeneuve, N. & Staudacher, T. (2007). Role of the structural inheritance of the oceanic lithosphere in the magmato-tectonic evolution of Piton de la Fournaise volcano (La Réunion Island). *Journal of Geophysical Research* **112**, doi:10.1029/2006JB004598.

Nimis, P. (1999). Clinopyroxene geobarometry of magmatic rocks. Part 2. Structural geobarometers for basic to acid, tholeiitic and mildly alkaline magmatic systems. *Contributions to Mineralogy and Petrology* **135**, 62–74.

Nercessian, A., Hirn, A., Lepine, J.-C. & Sapin, M. (1996). Internal structure of Piton de la Fournaise volcano from seismic wave propagation and earthquake distribution. *Journal of Volcanology and Geothermal Research* **70**, 123–143.

Peltier, A., Famin, V., Bachèlery, P., Cayol, V., Fukushima, Y. & Staudacher, T. (2008). Cyclic magma storages and transfers at Piton de la Fournaise volcano (La Réunion hotspot) inferred from deformation and geochemical data. *Earth and Planetary Science Letters* **270**, 180–188.

Peltier, A., Ferrazzini, V., Staudacher, T. & Bachèlery, P. (2005). Imaging the dynamics of dyke propagation prior to the 2000–2003 flank eruptions at Piton de La Fournaise, Réunion Island. *Geophysical Research Letters* **32**, 1–5.

Peltier, A., Staudacher, T. & Bachèlery, P. (2007). Constraints on magma transfers and structures involved in the 2003 activity at Piton de La Fournaise from displacement data. *Journal of Geophysical Research*, **112**, doi:10.1029/2006JB004379.

Roedder, P. L. & Emslie, R. F. (1970). Olivine-liquid equilibrium. *Contributions to Mineralogy and Petrology* **29**, 275–289.

Richet, P., Whittington, A., Holtz, F., Behrens, H., Ohlhorst, S. & Wilke, M. (2000). Water and the density of silicate glasses. *Contributions to Mineralogy and Petrology* **138**, 337–347.

Sapin, M., Hirn, A., Lepine, J.-C. & Nercessian, A. (1996). Stress, failure and fluid flow deduced from earthquakes accompanying eruptions at Piton de la Fournaise volcano. *Journal of Volcanology and Geothermal Research* **70**, 145–167.

Scarfe, C. M. & Cronin, D. J. (1986). Viscosity–temperature relationships of melts at 1 atm in the system diopside–albite. *American Mineralogist* **71**, 767–771.

Schwandt, C. S. & McKay, G. A. (2006). Minor- and trace-element sector zoning in synthetic enstatite. *American Mineralogist* **91**, 1607–1615.

Sigmundsson, F., Durand, P. & Massonnet, D. (1999). Opening of an eruptive fissure and seaward displacement at Piton de la Fournaise volcano measured by RADARSAT satellite radar interferometry. *Geophysical Research Letters* **26**, 533–536.

Sparks, R. S. J. & Huppert, H. E. (1984). Density changes during the fractional crystallization of basaltic magmas: Fluid dynamic implications. *Contributions to Mineralogy and Petrology* **85**, 300–309.

Stevenson, D. S. & Blake, S. (1998). Modelling the dynamics and thermodynamics of volcanic degassing. *Bulletin of Volcanology* **60**, 307–317.

Toplis, M. J. (2005). The thermodynamics of iron and magnesium partitioning between olivine and liquid: Criteria for assessing and predicting equilibrium in natural and experimental systems. *Contributions to Mineralogy and Petrology* **149**, 22–39.

Toutain, J.-P., Bachèlery, P., Blum, P.-A., Cheminée, J. L., Delorme, H., Fontaine, L., Kowalski, P. & Taochy, P. (1992). Real time monitoring of vertical ground deformations during eruptions at Piton de la Fournaise. *Geophysical Research Letters* **19**, 553–556.

Vlastélic, I., Staudacher, T. & Semet, M. (2005). Rapid change of lava composition from 1998 to 2002 at Piton de la Fournaise (Réunion) inferred from Pb isotopes and trace elements: evidence for variable crustal contamination. *Journal of Petrology* **46**, 79–107.

Vlastélic, I., Peltier, A. & Staudacher, T. (2007). Short-term (1998–2006) fluctuations of Pb isotopes at Piton de la Fournaise volcano (Réunion Island): origins and constraints on the size and shape of the magma reservoir. *Chemical Geology* **244**, 202–220.